

# Occam's Razor in Quark Mass Matrices

Morimitsu Tanimoto<sup>1</sup>    and    Tsutomu T. Yanagida<sup>2</sup>

<sup>1</sup>*Department of Physics, Niigata University, Niigata 950-2181, Japan*

<sup>2</sup>*Kavli IPMU, TODIAS, University of Tokyo, Kashiwa 277-8583, Japan*

## Abstract

On the standpoint of Occam's Razor approach, we consider the minimum number of parameters in the quark mass matrices needed for the successful CKM mixing and CP violation. We impose three zeros in the down-quark mass matrix with taking the diagonal up-quark mass matrix to reduce the number of free parameters. The three zeros are maximal zeros in order to have a CP violating phase in the quark mass matrix. Then, there remain six real parameters and one CP violating phase, which is the minimal number to reproduce the observed data of the down-quark masses and the CKM parameters. The twenty textures with three zeros are examined. Among them, the thirteen textures are viable for the down-quark mass matrix. As a representative of these textures, we discuss a texture  $M_d^{(1)}$  in details. By using the experimental data on  $\sin 2\beta$ ,  $\theta_{13}$  and  $\theta_{23}$  together with the observed quark masses, the Cabibbo angle is predicted to be close to the experimental data. It is found that this surprising result remains unchanged in all other viable textures. We also investigate the correlations among  $|V_{ub}/V_{cb}|$ ,  $\sin 2\beta$  and  $J_{CP}$ . For all textures, the maximal value of the ratio  $|V_{ub}/V_{cb}|$  is 0.09, which is smaller than the upper-bound of the experimental data, 0.094. We hope that this prediction will be tested in future experiments.

# 1 Introduction

The standard model is now well established by the recent discovery of the Higgs boson. In spite of the success of the standard model, underlying physics determining the quark and lepton mass matrices is still unknown. Because of this there have been proposed a number of models based on flavor symmetries, but no convincing model has been proposed.

A long times ago, Weinberg [1] considered a mass matrix for the down-quark sector in the basis of the up-quark mass matrix being diagonal. He assumed a vanishing (1,1) element in the  $2 \times 2$  matrix and imposed a symmetric form of the matrix in order to reduce the number of free parameters. Then, the number of free parameters is reduced to only two and hence he succeeded to predict the Cabibbo angle to be  $\sqrt{m_d/m_s}$ , which is very successful and called as the Gatto, Sartori, Tonin relation [2].<sup>1</sup>

The success of the Weinberg approach encouraged many authors to consider various flavor symmetries in the quark matrices by extending it to the three family case. In this paper, however, we point out that the Cabibbo angle is predicted successfully in the framework of “Occam’s Razor” approach proposed in the lepton sector [6].<sup>2</sup> In other word, we show that the Weinberg matrix can be obtained without any symmetry.

On the standpoint of Occam’s Razor approach, we consider the minimum number of parameters needed for the successful CKM mixing and CP violation without assuming the symmetric or hermitian mass matrix of down quarks. We impose three zeros in the down-quark mass matrix. We always take the up-quark mass matrix to be diagonal since we do not need any off-diagonal element to explain the observation. Therefore, the down-quark mass matrix is given with six complex parameters. Among them, five phases can be removed by the phase redefinition of the three right-handed and three left-handed down quark fields. After the field-phase rotation, there remain six real parameters and one CP violating phase, which are the minimal number to reproduce the seven observed data, that is the three down-quark masses and the four CKM parameters. It is emphasized that the three-zero texture keeps one CP violating phase in the down-quark mass matrix. In the present Occam’s Razor approach with three families, we show that the successful prediction of the Cabibbo angle is obtained. It is surprising that the Weinberg’s ansatz, that is (1, 2) and (2, 1) elements to be symmetric, is derived in our Occam’s Razor approach.

In order to reproduce the bottom-quark mass and the CKM mixing angles,  $V_{us}$  and  $V_{cb}$ , we take the elements (3, 3), (2, 3), (1, 2) of the  $3 \times 3$  down-quark mass matrix to be non-vanishing. Then, we have  ${}_6C_3 = 20$  textures with three zeros. For our convenience, we classify them in two categories; (A) where a (2, 2) element is non-vanishing and (B) where a (2, 2) element is vanishing. In the category (A), the six textures with three zeros are

---

<sup>1</sup> Fritzsch extended the above approach to the three family case [3, 4]. He set four zeros in each down-quark and up-quark mass matrices, which are both symmetric. Then, there were eight parameters against the ten observed data. However, it was ruled out by the observed CKM element  $V_{cb}$ . Ramond, Roberts and Ross also presented the systematic work with four or five zeros for the symmetric or hermitian quark mass matrix [5]. Their textures are also not viable under the precise experimental data at present, because four or five zeros is too tight to reproduce the ten observed data.

<sup>2</sup> The Occam’s Razor approach predicts the CP-violating phase  $\delta = \pm\pi/2$  in the neutrino oscillation. It is very much interesting that one of the predictions,  $\delta \simeq -\pi/2$ , is favored in a global analysis of the neutrino oscillation data [7].

viable for the down-quark mass matrix. In the category (B), there are seven viable textures with three zeros. Finally, we have found that those thirteen textures are all consistent with the present experimental data on quark masses and the CKM parameters. However, we should note that some textures are equivalent each other due to the freedom of the unitary transformation of the right-handed down quarks.

In section 2, we show viable down-quark mass matrices with three zeros in the categories (A) and (B), and explain how to obtain the CKM mixing angles and the CP violating phase. In section 3, we show numerical results for those mass matrices. The discussion and summary is devoted in section 4. In Appendices A and B, we show unfavored down-quark mass matrices and the above redundancy of our textures, respectively.

## 2 Quark mass matrix in the Occam's Razor approach

### 2.1 Three texture zeros for down-quarks

Let us discuss the down-quark mass matrix. We always take the basis where the up-quark mass matrix is diagonal. The number of free parameters in the down-quark mass matrix is reduced by putting zero at several elements in the matrix. We consider the three texture zeros, which provide the minimum number of parameters needed for the successful CKM mixing and CP violation. We never assume any flavor symmetry. We call this as ‘‘Occam’s Razor’’ approach.

Before investigating the quark mass matrix, we present our setup in more details. The Lagrangian for the quark Yukawa sector is given by

$$\mathcal{L}_Y = y_{\alpha\beta}^u \bar{Q}_{L\alpha} u_{R\beta} \tilde{h} + y_{\alpha\beta}^d \bar{Q}_{L\alpha} d_{R\beta} h , \quad (1)$$

where  $Q_{L\alpha}$ ,  $u_{R\beta}$ ,  $d_{R\beta}$  and  $h$  denote the left-handed quark doublets, the right-handed up-quark singlet, the right-handed down-quark singlet, and the Higgs doublet, respectively. The quark mass matrices are given as  $m_{\alpha\beta} = y_{\alpha\beta} v_H$  with  $v_H = 174.104$  GeV. In order to reproduce the observed quark masses and the CKM matrix with the minimal number of parameters, we take the diagonal basis in the up-quark sector,

$$M_u = \begin{pmatrix} m_u & 0 & 0 \\ 0 & m_c & 0 \\ 0 & 0 & m_t \end{pmatrix}_{LR} . \quad (2)$$

For the down-quark mass matrix, we impose the three texture zeros. Then, the texture of the down-quark mass matrix  $M_d$  is given with six complex parameters. The five phases can be removed by the phase rotation of the three right-handed and three left-handed down-quark fields. Therefore, there remains six real parameters and one CP violating phase, which are the minimal number to reproduce the observed data of masses and the CKM parameters.

Now, we can discuss textures for the down-quark mass matrix. Let us start with taking (3, 3), (2, 3), (1, 2) elements of  $M_d$  to be non-vanishing values to reproduce the observed

bottom quark mass and the CKM mixing angles,  $V_{us}$  and  $V_{cb}$ .<sup>3</sup> Then, we have  ${}_6C_3 = 20$  textures with three zeros for the down-quark mass matrix. For our convenience, we classify them in two categories, (A) and (B), as explained in the introduction. In (A), we have  ${}_5C_2 = 10$  textures with a non-vanishing  $(2, 2)$  element and in (B) we have also ten textures with a vanishing  $(2, 2)$  element.

We first discuss textures in the category (A). The ten textures are written as follows:

$$\begin{aligned} & \begin{pmatrix} 0 & A & 0 \\ A' & B & C \\ 0 & C' & D \end{pmatrix}, \quad \begin{pmatrix} A' & A & 0 \\ 0 & B & C \\ 0 & C' & D \end{pmatrix}, \quad \begin{pmatrix} 0 & A & 0 \\ 0 & B & C \\ A' & C' & D \end{pmatrix}, \quad \begin{pmatrix} 0 & A & C' \\ A' & B & C \\ 0 & 0 & D \end{pmatrix}, \quad \begin{pmatrix} A' & A & C' \\ 0 & B & C \\ 0 & 0 & D \end{pmatrix}, \\ & \begin{pmatrix} 0 & A & C' \\ 0 & B & C \\ A' & 0 & D \end{pmatrix}, \quad \begin{pmatrix} 0 & A & 0 \\ A' & B & C \\ C' & 0 & D \end{pmatrix}, \quad \begin{pmatrix} A' & A & 0 \\ C' & B & C \\ 0 & 0 & D \end{pmatrix}, \quad \begin{pmatrix} 0 & A & C' \\ 0 & B & C \\ 0 & A' & D \end{pmatrix}, \quad \begin{pmatrix} A' & A & 0 \\ 0 & B & C \\ C' & 0 & D \end{pmatrix}, \end{aligned} \quad (3)$$

where  $A, A', B, C, C'$  and  $D$  are complex parameters. We will show that the first six textures are consistent with the present experimental data. Those six down-quark mass matrices are parametrized after removing five phases by the phase rotation of quark fields as follows:

$$\begin{aligned} M_d^{(1)} &= \begin{pmatrix} 0 & a & 0 \\ a' & b e^{-i\phi} & c \\ 0 & c' & d \end{pmatrix}_{LR}, \quad M_d^{(2)} = \begin{pmatrix} a' & a & 0 \\ 0 & b e^{-i\phi} & c \\ 0 & c' & d \end{pmatrix}_{LR}, \quad M_d^{(3)} = \begin{pmatrix} 0 & a & 0 \\ 0 & b e^{-i\phi} & c \\ a' & c' & d \end{pmatrix}_{LR}, \\ M_d^{(4)} &= \begin{pmatrix} 0 & a & c' \\ a' & b e^{-i\phi} & c \\ 0 & 0 & d \end{pmatrix}_{LR}, \quad M_d^{(5)} = \begin{pmatrix} a' & a & c' \\ 0 & b e^{-i\phi} & c \\ 0 & 0 & d \end{pmatrix}_{LR}, \quad M_d^{(6)} = \begin{pmatrix} 0 & a & c' \\ 0 & b e^{-i\phi} & c \\ a' & 0 & d \end{pmatrix}_{LR}, \end{aligned} \quad (4)$$

where  $a, a', b, c, c'$  and  $d$  are real parameters, and  $\phi$  is the CP violating phase. It should be stressed that our matrices are not symmetric at all. The CP violating phase  $\phi$  is put in the  $(2, 2)$  entry.<sup>4</sup> In the next section, we examine those seven parameters numerically to reproduce the three down quark masses, three CKM mixing angles and one CP violating phase.

We discuss briefly why the last four textures (seventh-tenth ones) in Eq.(3) are excluded by the experimental data. The seventh and eighth textures in Eq.(3) give a vanishing CKM mixing angle. The ninth one gives us one massless quark because the first column is a zero vector in the flavor space. The last one cannot reproduce the magnitude of the CP violation. The details are shown in Appendix A.

---

<sup>3</sup>By the unitary transformation of the right-handed quarks, we can move to textures with other non-vanishing entries.

<sup>4</sup>One can put  $\phi$  in other places without changing the predicted mass eigenvalues and CKM elements since the rephasing is possible in these mass matrices.

Now, we discuss textures in the category (B), in which the  $(2, 2)$  element is zero. We can write the ten textures as follows:

$$\begin{aligned}
& \begin{pmatrix} A' & A & B \\ 0 & 0 & C \\ 0 & C' & D \end{pmatrix}, \quad \begin{pmatrix} 0 & A & B \\ A' & 0 & C \\ 0 & C' & D \end{pmatrix}, \quad \begin{pmatrix} 0 & A & B \\ 0 & 0 & C \\ A' & C' & D \end{pmatrix}, \quad \begin{pmatrix} A & A' & C' \\ B & 0 & C \\ 0 & 0 & D \end{pmatrix}, \quad \begin{pmatrix} A & A' & B \\ 0 & 0 & C \\ C' & 0 & D \end{pmatrix}, \\
& \begin{pmatrix} 0 & A & B \\ A' & 0 & C \\ C' & 0 & D \end{pmatrix}, \quad \begin{pmatrix} A & A' & 0 \\ B & 0 & C \\ C' & 0 & D \end{pmatrix}, \quad \begin{pmatrix} A' & A & 0 \\ 0 & 0 & C \\ B & C' & D \end{pmatrix}, \quad \begin{pmatrix} 0 & A & 0 \\ A' & 0 & C \\ B & C' & D \end{pmatrix}, \quad \begin{pmatrix} A' & A & 0 \\ B & 0 & C \\ 0 & C' & D \end{pmatrix}.
\end{aligned} \tag{5}$$

The first seven textures are also consistent with the present experimental data. After removing five phases by the phase rotation of quark fields, those seven down-quark mass matrices are parametrized as:

$$\begin{aligned}
M_d^{(11)} &= \begin{pmatrix} a' & a e^{-i\phi} & b \\ 0 & 0 & c \\ 0 & c' & d \end{pmatrix}_{LR}, \quad M_d^{(12)} = \begin{pmatrix} 0 & a e^{-i\phi} & b \\ a' & 0 & c \\ 0 & c' & d \end{pmatrix}_{LR}, \quad M_d^{(13)} = \begin{pmatrix} 0 & a e^{-i\phi} & b \\ 0 & 0 & c \\ a' & c' & d \end{pmatrix}_{LR}, \\
M_d^{(14)} &= \begin{pmatrix} a e^{i\phi} & a' & c' \\ b & 0 & c \\ 0 & 0 & d \end{pmatrix}_{LR}, \quad M_d^{(15)} = \begin{pmatrix} a e^{-i\phi} & a' & b \\ 0 & 0 & c \\ c' & 0 & d \end{pmatrix}_{LR}, \\
M_d^{(16)} &= \begin{pmatrix} 0 & a & b \\ a' & 0 & c e^{-i\phi} \\ c' & 0 & d \end{pmatrix}_{LR}, \quad M_d^{(17)} = \begin{pmatrix} a & a' & 0 \\ b & 0 & c e^{i\phi} \\ c' & 0 & d \end{pmatrix}_{LR}.
\end{aligned} \tag{6}$$

The last three textures (eighth-tenth ones) in Eq.(5) are also excluded by the experimental data. The eighth and ninth textures in Eq.(5) give a vanishing CKM mixing angle. The tenth ones cannot reproduce the magnitudes of the CP violation. The details are discussed in Appendix A.

Finally, we comment on the freedoms of the unitary transformation of the right-handed quarks. Since the CKM matrix is the flavor mixing among the left-handed quarks, some textures in Eqs.(4) and (6) are equivalent each other due to the freedom of the unitary transformation of the right-handed quarks. We show the redundancy among them in Appendix B.

## 2.2 CKM parameters for $M_d^{(1)}$

Let us show how to predict the CKM mixing angles and the CP violation taking the case of  $M_d^{(1)}$  in Eq.(4) as a representative. Since the up-type quark mass matrix is diagonal, the

CKM matrix is obtained by diagonalizing the down-quark mass matrix  $M_d^{(1)}$ . In order to determine the left-handed quark mixing angles, we study  $M_d^{(1)} M_d^{(1)\dagger}$ ;

$$M_d^{(1)} M_d^{(1)\dagger} = \begin{pmatrix} a^2 & ab e^{i\phi} & ac' \\ ab e^{-i\phi} & a'^2 + b^2 + c^2 & bc' e^{-i\phi} + cd \\ ac' & bc' e^{i\phi} + cd & c'^2 + d^2 \end{pmatrix}_{LL}. \quad (7)$$

By solving the eigenvalue equation of  $M_d^{(1)} M_d^{(1)\dagger}$ , we obtain

$$\begin{aligned} m_d^2 + m_s^2 + m_b^2 &= a^2 + a'^2 + b^2 + c^2 + c'^2 + d^2, \\ m_d^2 m_s^2 + m_s^2 m_b^2 + m_b^2 m_d^2 &= a^2 a'^2 + a^2 (c^2 + d^2) + a'^2 (c'^2 + d^2) + c^2 c'^2 + b^2 d^2 - 2bcc'd \cos \phi, \\ m_d^2 m_s^2 m_b^2 &= a^2 a'^2 d^2. \end{aligned} \quad (8)$$

On the other hand, the eigenvectors lead to the CKM elements  $V_{ij}$  and the CKM phase  $\delta_{CP}$ , which is given in the PDG parametrization [8]. Those are given in the leading order as follows:

$$|V_{us}| \simeq \frac{ab}{m_s^2} \left| \sin \frac{\phi}{2} \right|, \quad |V_{cb}| \simeq \sqrt{2} \frac{c}{m_b} \left| \cos \frac{\phi}{2} \right|, \quad |V_{ub}| \simeq \frac{ac'}{m_b^2}, \quad \delta_{CP} \simeq \frac{1}{2}(\pi - \phi), \quad (9)$$

where we adopt the approximate relations  $b \sim c$  and  $c' \sim d$ , which will be justified in our numerical results.

Although the source of the CP violation is only one, we have various measurements of the CP violating phase. We can also define the other CP violating quantity,  $\beta$  (or  $\phi_1$ ), which is the one angle of the unitarity triangle:

$$\beta (\phi_1) = \arg \left( -\frac{V_{cd} V_{cb}^*}{V_{td} V_{tb}^*} \right). \quad (10)$$

Actually,  $\sin 2\beta$  has been measured precisely in the B-factory [8]. It is given concisely in the leading order by

$$\sin 2\beta \simeq \sin \phi. \quad (11)$$

There is another CP violating observable, the Jarlskog invariant  $J_{CP}$  [9], which is derived from the following relation:

$$\begin{aligned} iC &\equiv [M_u M_u^\dagger, M_d M_d^\dagger], \\ \det C &= -2J_{CP}(m_t^2 - m_c^2)(m_c^2 - m_u^2)(m_u^2 - m_t^2)(m_b^2 - m_s^2)(m_s^2 - m_d^2)(m_d^2 - m_b^2). \end{aligned} \quad (12)$$

The predicted one is exactly expressed in terms of the parameters of the mass matrix elements as:

$$J_{CP} = \frac{-1}{(m_b^2 - m_s^2)(m_s^2 - m_d^2)(m_d^2 - m_b^2)} j_{CP}, \quad (13)$$

where

$$j_{CP} = a^2 b c c' d \sin \phi. \quad (14)$$

For  $M_d^{(k)}$  ( $k = 1 - 6$ ) and  $M_d^{(k)}$  ( $k = 11 - 17$ ), we summarize three CKM elements  $V_{ij}$ , the CP violating phase  $\delta_{CP}$  and  $j_{CP}$  in Table 1.

	$ V_{us} $	$ V_{cb} $	$ V_{ub} $	$\delta_{CP}$	$j_{CP}$
$M_d^{(1)}, M_d^{(2)}, M_d^{(3)}, M_d^{(16)}, M_d^{(17)}$	$\frac{ab}{m_s^2} \left  \sin \frac{\phi}{2} \right $	$\frac{\sqrt{2}c}{m_b} \left  \cos \frac{\phi}{2} \right $	$\frac{ac'}{m_b^2}$	$\frac{1}{2}(\pi - \phi)$	$a^2bcc'd \sin \phi$
$M_d^{(4)}, M_d^{(5)}, M_d^{(6)}, M_d^{(14)}$	$\frac{ab}{m_s^2}$	$\frac{c}{m_b}$	$\frac{c'}{m_b}$	$\phi$	$abcc'd^2 \sin \phi$
$M_d^{(11)}, M_d^{(12)}, M_d^{(13)}, M_d^{(15)}$	$\frac{ac}{m_s^2} \frac{c'}{m_b}$	$\frac{c}{m_b}$	$\frac{b}{m_b}$	$\pi - \phi$	$abc^2c'd \sin \phi$

Table 1: The predicted CKM elements, the CP phase and the CP violating measure  $j_{CP}$ , where  $|V_{ij}|$  and  $\delta_{CP}$  are given in the leading order, and  $j_{CP}$  is the exact one.

### 3 Numerical studies of Textures

#### 3.1 Derivation of Weinberg's mass matrix for $M_d^{(1)}$

Since the texture of  $M_d^{(1)}$  is the most familiar one among the thirteen textures in Eqs.(4) and Eq.(6), we show how to obtain the numerical result by taking  $M_d^{(1)}$  as a typical representative. In order to reduce the number of the free parameters, we use the three observed down-quark masses as inputs. We adopt the data of the down-quark Yukawa couplings at the  $M_Z$  scale [10] as

$$y_d = (1.58_{-0.10}^{+0.23}) \times 10^{-5}, \quad y_s = (3.12_{-0.16}^{+0.17}) \times 10^{-4}, \quad y_b = (1.639 \pm 0.015) \times 10^{-2}, \quad (15)$$

which give quark masses as  $m_q = y_q v_H$  with  $v_H = 174.104$  GeV. For  $M_d^{(1)}$ , it is convenient to eliminate the parameters  $a', d$  and  $\phi$  by using Eq.(8), where the three quark masses in Eq.(15) are put at the 90% C.L, respectively. Then, there remain four parameters  $a, b, c$  and  $c'$ . We calculate the CKM parameters by scanning these parameters randomly in the region of  $\{a, b, c, c', d\} = \{0, m_b\}$  with  $a, b, c, c' \leq d$ .

In fig.1, we show the frequency distribution of the predicted value of  $|V_{us}|$ . The large angle is allowed as well as the small angle with almost same weight. In fig.2, we show the  $|V_{us}|$  versus  $a/a'$ . Since we do not assume any relation among the parameters  $a, b, c$  and  $c'$ , the larger values than  $1/\sqrt{2}$  are allowed. The observed Cabibbo angle favors around  $a/a' = 1$ , which was assumed in the Weinberg's approach. Since we do not assume  $a/a' = 1$ , the allowed  $|V_{us}|$  lies in  $0 - 1$  at this stage. We will show that the desired relation  $a/a' \simeq 1$  is finally derived without using the observed Cabibbo angle in our approach.

In figs.3 and 4, we show the frequency distributions of the predicted value of  $|V_{cb}|$  and  $|V_{ub}|$ , respectively. The  $|V_{cb}|$  is allowed up to the maximal mixing  $1/\sqrt{2}$ . On the other hand, the  $|V_{ub}|$  is predicted to be smaller than 0.02 because of the quark mass hierarchy as seen in Eqs.(8) and (9). However, it is still much larger than the observed value.

Here, we show the present experimental data on the CKM mixing angles and the CP

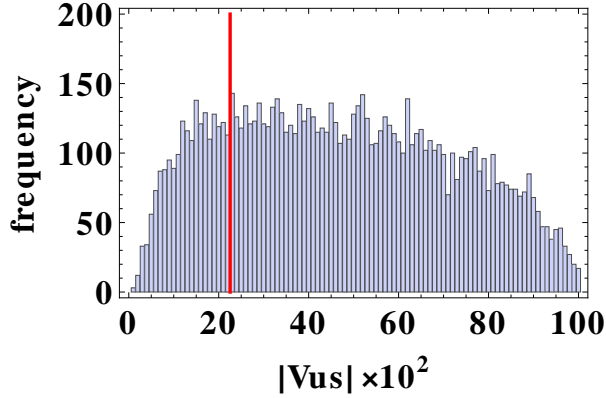


Figure 1: The frequency distribution of the predicted  $|V_{us}|$  in arbitrary unit without the CKM constraints for  $M_d^{(1)}$ . The red line denotes the experimental value.

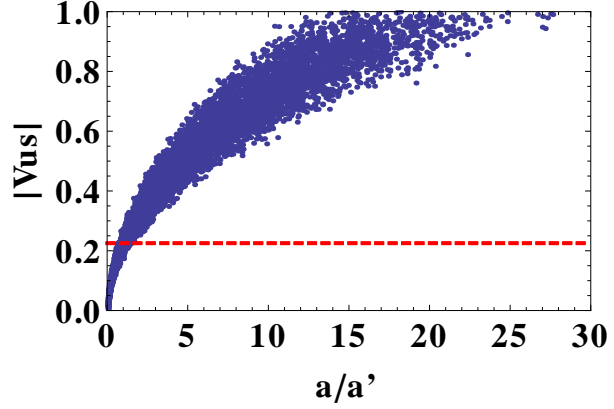


Figure 2: The prediction of  $|V_{us}|$  versus  $a/a'$  without the CKM constraints for  $M_d^{(1)}$ . The red dashed line denotes the experimental value.

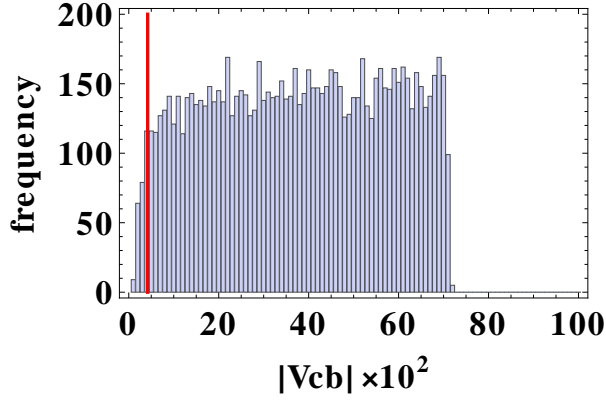


Figure 3: The frequency distribution of the predicted  $|V_{cb}|$  in arbitrary unit without the CKM constraints for  $M_d^{(1)}$ . The red line denotes the experimental value.

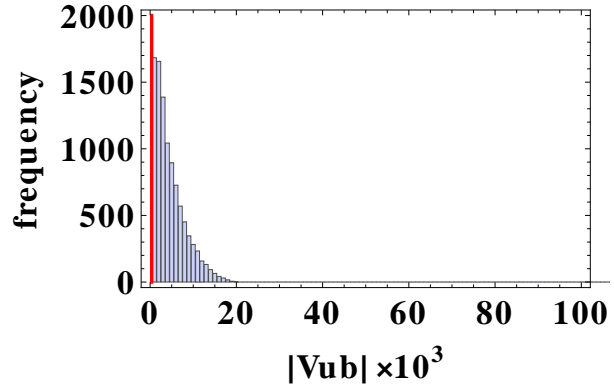


Figure 4: The frequency distribution of the predicted  $|V_{ub}|$  in arbitrary unit without the CKM constraints for  $M_d^{(1)}$ . The red line denotes the experimental value.

violating phase at the  $M_Z$  scale [10],

$$\begin{aligned} \theta_{12} &= 0.22735 \pm 0.00072, & \theta_{23} &= (4.208 \pm 0.064) \times 10^{-2}, \\ \theta_{13} &= (3.64 \pm 0.13) \times 10^{-3}, & \delta_{CP} &= 1.208 \pm 0.054 \text{ [rad]}, \end{aligned} \quad (16)$$

where  $\theta_{ij}$  is defined in the PDG parametrization [8]. We can also use the other CP violating measure,  $\sin 2\beta$ , as an input parameter. The experimental data on  $\sin 2\beta$  is given by [8]:

$$\sin 2\beta = 0.682 \pm 0.019. \quad (17)$$

We will discuss the predicted  $J_{CP}$  comparing with the experimental data,

$$J_{CP} = (3.06^{+0.21}_{-0.20}) \times 10^{-5}, \quad (18)$$



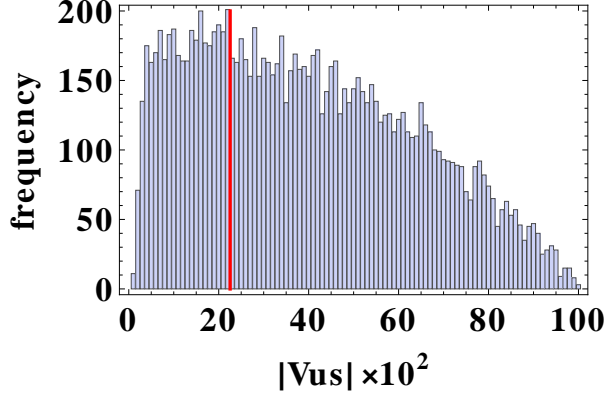


Figure 5: The frequency distribution of  $|V_{us}|$  in arbitrary unit with the constraint of  $\sin 2\beta$  for  $M_d^{(1)}$ . The red line denotes the experimental value.

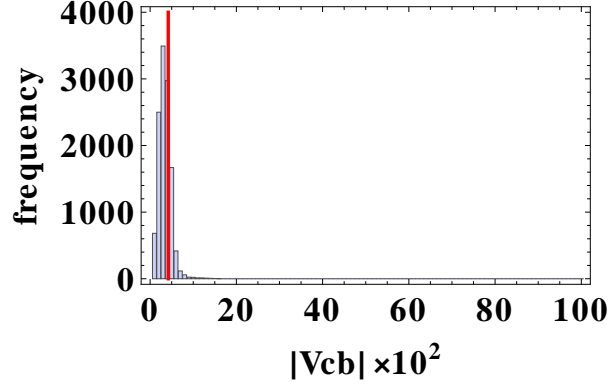


Figure 6: The frequency distribution of  $|V_{cb}|$  in arbitrary unit with the constraint of  $\sin 2\beta$  for  $M_d^{(1)}$ . The red line denotes the experimental value.

which is obtained by the global fit of the CKM parameters [8].

Let us, first, use the CP violating phase in addition to the three quark masses. We adopt the observed data on  $\sin 2\beta$  in Eq.(17), which is more sensitive to constrain the parameters compared with the data on  $\delta_{CP}$ . In figs.5 and 6, we show the frequency distributions of the predicted values of  $|V_{us}|$  and  $|V_{cb}|$ , respectively. The predicted  $|V_{us}|$  is still broad as  $0 - 1$ . However, the frequency distribution of  $|V_{cb}|$  is impressive because the peak is very sharp around the observed value. Thank to the constraint of the experimental data of  $\sin 2\beta$ , the predicted  $|V_{cb}|$  is restricted to be in the narrow region at one push. In fig.7, we show the frequency distribution of the predicted value of  $|V_{ub}|$ . This distribution is not much changed compared with the case in fig.4.

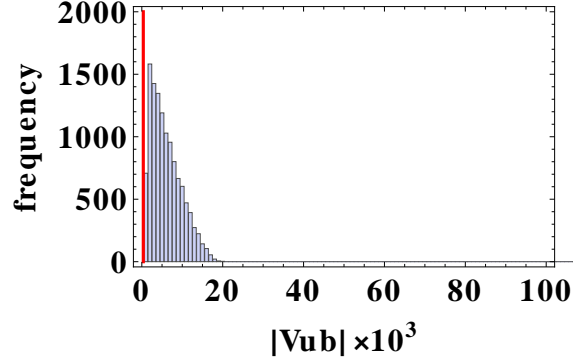


Figure 7: The frequency distribution of  $|V_{ub}|$  in arbitrary unit with the constraint of  $\sin 2\beta$  for  $M_d^{(1)}$ . The red line denotes the experimental value.

In the next step, we add the constraint of the experimental data  $\theta_{13}$  in Eq.(16). In fig.8, we show the frequency distribution for the predicted value of  $|V_{us}|$ . The peak of this distribution is around the experimental value although the large mixing is still allowed. The frequency distribution of the predicted value of  $|V_{cb}|$  is presented in fig.9. This distribution is not much changed compared with the case in fig.6.

At the last step, we impose the constraint of the experimental data  $\theta_{23}$  in Eq.(16). Then, we obtain the predicted Cabibbo angle with a good accuracy. In fig.10, the frequency distribution of the predicted value of  $|V_{us}|$  is shown. The predicted  $|V_{us}|$  is shown versus the parameter  $a/a'$  in fig.11. The prediction is completely consistent with the experimental data,

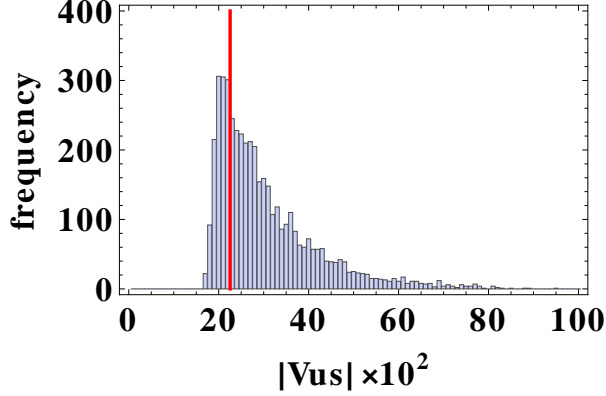


Figure 8: The frequency of  $|V_{us}|$  in arbitrary unit with the constraints of  $\sin 2\beta$  and  $|V_{ub}|$  for  $M_d^{(1)}$ . The red line denotes the experimental value.

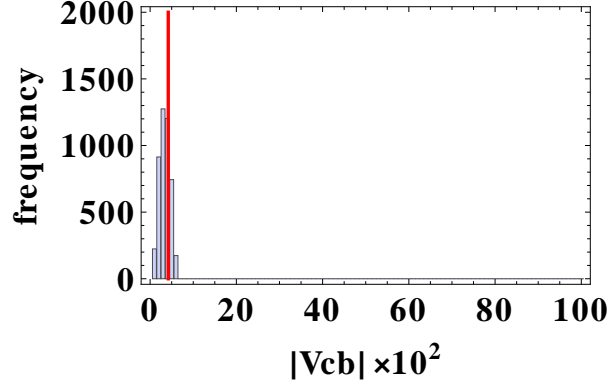


Figure 9: The frequency of  $|V_{cb}|$  in arbitrary unit with the constraints of  $\sin 2\beta$  and  $|V_{ub}|$  for  $M_d^{(1)}$ . The red line denotes the experimental value.

and the ratio  $a/a' = 0.7 - 1.9$  is given. Thus, the Weinberg's ansatz  $a/a' = 1$  is obtained by using the experimental data  $\sin 2\beta$ ,  $\theta_{13}$  and  $\theta_{23}$  without assuming any flavor symmetry. Now, we can determine the parameter  $a$  (or  $a/a'$ ) precisely by using the experimental data  $\theta_{12}$  in Eq.(16).

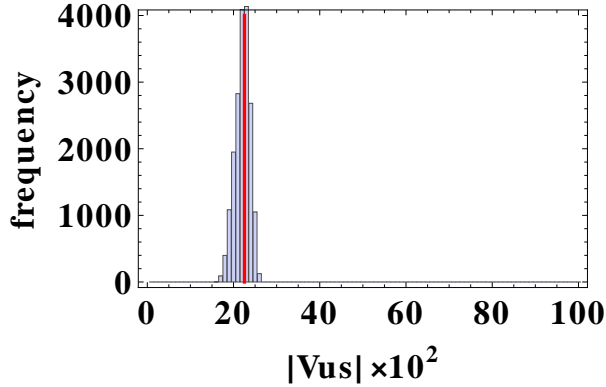


Figure 10: The frequency of  $|V_{us}|$  in arbitrary unit with the constraints of  $\sin 2\beta$ ,  $|V_{ub}|$  and  $|V_{cb}|$  for  $M_d^{(1)}$ . The red line denotes the experimental value.

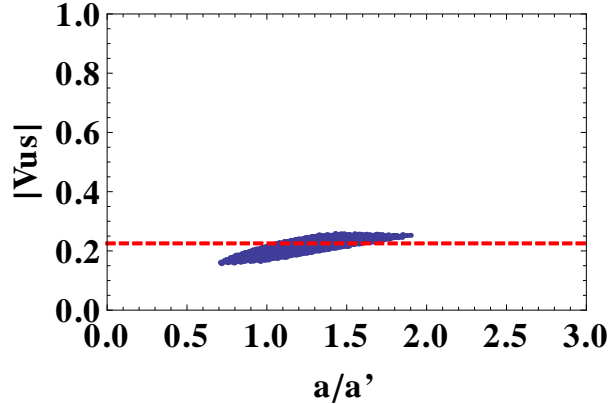


Figure 11: The prediction of  $|V_{us}|$  versus  $a/a'$  with the constraints of  $\sin 2\beta$ ,  $|V_{ub}|$  and  $|V_{cb}|$  for  $M_d^{(1)}$ . The red dashed line denotes the experimental value.

The seven parameters of  $M_d^{(1)}$  are determined completely by the experimental data. However, we can add further investigations since there is still large error-bars in the experimental data  $|V_{ub}|$ . We show the predicted ratio  $|V_{ub}/V_{cb}|$  versus  $\sin 2\beta$  in fig.12. The upper bound of the predicted ratio is 0.09 while the experimental data allows up to 0.094. Thus, the precise measurements of the ratio  $|V_{ub}/V_{cb}|$  and  $\sin 2\beta$  are a crucial test of our textures.

There is another CP violating parameter  $J_{CP}$  in addition to  $\sin 2\beta$  and  $\delta_{CP}$ . We also show

the predicted  $J_{CP}$  versus  $|V_{ub}|$  in fig.13, where the red dashed lines denote experimental bounds in Eqs. (16) and (17). The some experimental allowed region is excluded in our texture. The precise measurements of  $|V_{ub}|$  and  $J_{CP}$  also provide us a test of our textures.

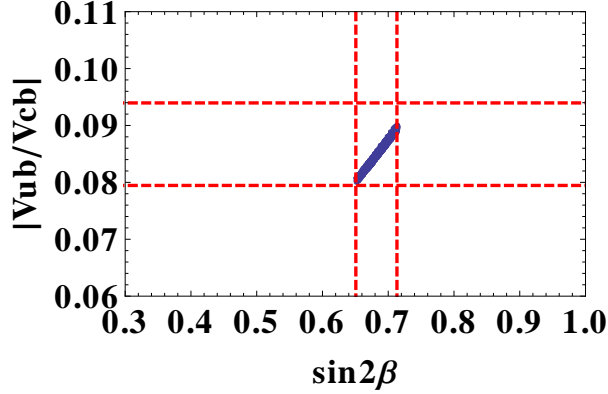


Figure 12: The predicted ratio  $|V_{ub}|/|V_{cb}|$  versus  $\sin 2\beta$  in  $M_d^{(1)}$ . The red dashed lines denote the upper and lower bounds of the experimental data with 90% C.L.

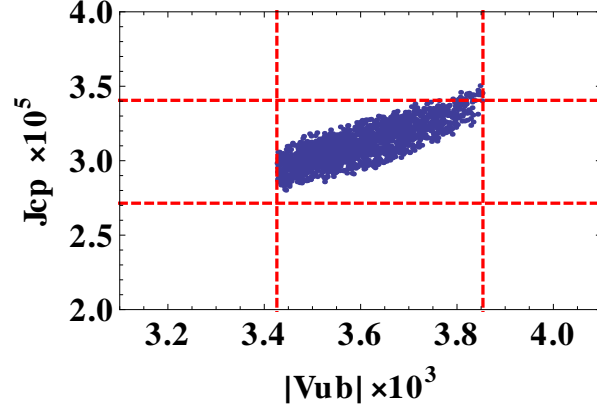


Figure 13: The predicted  $J_{CP}$  versus  $|V_{ub}|$  in  $M_d^{(1)}$ . The red dashed lines denote the upper and lower bounds of the experimental data with 90% C.L.

### 3.2 Other textures $M_d^{(k)}$ ( $k = 2 - 6, 11 - 17$ )

The predictions of the mixing angles and the CP violating phase in our thirteen textures are classified in the three groups as seen in Table 1. The predictions of the first group have been presented for  $M_d^{(1)}$  in the previous subsection. Other mass matrices  $M_d^{(k)}$  ( $k = 2 - 6, 11 - 17$ ) can be also studied in the same way. We have checked numerically that the Cabibbo angle is predicted with a good accuracy by using the experimental data  $\sin 2\beta$ ,  $\theta_{13}$  and  $\theta_{23}$  without assuming any flavor symmetry. We summarize the allowed region of the parameters in Table 2 and Table 3, where  $M_d^{(16)}$  is the exceptional case with  $c' > d$ . We have found that only six textures are independent among thirteen textures as shown in Appendix B.

	$a$ [MeV]	$a'$ [MeV]	$b$ [MeV]	$c$ [MeV]	$c'$ [GeV]	$d$ [GeV]	$\phi$ [°]
$M_d^{(1)}$	15-17.5	10-15	92-104	78-95	1.65-2.0	2.0-2.3	37-48
$M_d^{(2)}$	15-17	2-4	94-106	78-95	1.65-2.0	2.0-2.3	40-49
$M_d^{(3)}$	15-17.5	250-380	92-104	78-95	1.65-2.0	2.0-2.3	37-48
$M_d^{(4)}$	11-14	9-17	45-58	115-128	0.009-0.011	2.8-2.9	63-75
$M_d^{(5)}$	11-14	2-4	45-58	115-128	0.009-0.011	2.8-2.9	63-75
$M_d^{(6)}$	11-14	220-420	45-58	115-128	0.009-0.011	2.8-2.9	63-75

Table 2: The allowed regions of parameters for each  $M_d^{(k)}$  ( $k = 1 - 6$ ).

	$a$ [MeV]	$a'$ [MeV]	$b$ [MeV]	$c$ [MeV]	$c'$ [GeV]	$d$ [GeV]	$\phi$ [°]
$M_d^{(11)}$	10-12	2.5-3.5	11-13	125-135	1.0-1.2	2.5-2.7	104-118
$M_d^{(12)}$	10-12	11-18	11-13	125-135	1.0-1.2	2.5-2.7	106-120
$M_d^{(13)}$	10-12	260-390	11-13	125-135	1.0-1.2	2.5-2.7	104-118
$M_d^{(14)}$	11-14	2-4	45-58	115-128	0.009-0.011	2.8-2.9	63-75
$M_d^{(15)}$	10-12	2.5-3.5	11-13	125-135	1.0-1.2	2.5-2.7	104-118
$M_d^{(16)}$	2-4	78-95	15-17	94-106	2.0-2.3	1.65-2.0	40-49
$M_d^{(17)}$	15-17	2-4	94-106	78-95	1.65-2.0	2.0-2.3	40-49

Table 3: The allowed regions of parameters for each  $M_d^{(k)}$  ( $k = 11 - 17$ ).

We show here predictions for  $M_d^{(5)}$  and  $M_d^{(11)}$  since numerical results are almost the same in the same group in Table 1. In fig.14, we show the predicted ratio  $|V_{ub}/V_{cb}|$  versus  $\sin 2\beta$  for  $M_d^{(5)}$  as a representative of the second group in Table 1. The upper bound of the predicted ratio is also 0.09, which is the same as the one in fig.12 for  $M_d^{(1)}$ . The prediction is smaller than the experimental upper bound 0.094. We show the  $J_{CP}$  versus  $|V_{ub}|$  in fig.15 for  $M_d^{(5)}$ , where the red dashed lines denote experimental bounds in Eqs. (16) and (17). The predicted  $J_{CP}$  is different from the one in fig.13 for  $M_d^{(1)}$ .

In fig.16, we show the predicted ratio  $|V_{ub}/V_{cb}|$  versus  $\sin 2\beta$  for  $M_d^{(11)}$  as a representative of the third group in Table 1. The prediction is the same as the one for  $M_d^{(1)}$  and  $M_d^{(5)}$  as seen in figs.12 and 14. We show the  $J_{CP}$  versus  $|V_{ub}|$  for  $M_d^{(11)}$  in fig.17. The predicted  $J_{CP}$  is almost the same as the one in fig.13, but different from the one in fig. 15. Therefore, the precise measurements of  $|V_{ub}/V_{cb}|$ ,  $J_{CP}$  and  $\sin 2\beta$  are important to distinguish the textures.

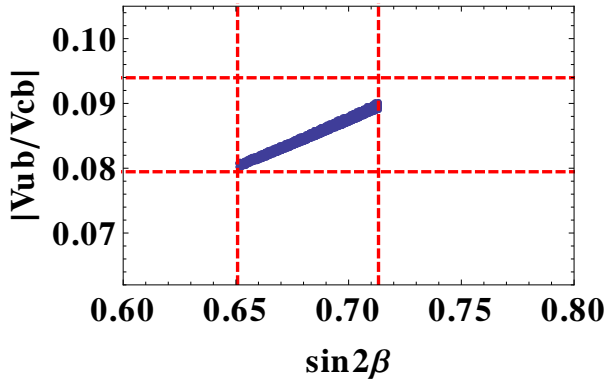


Figure 14: The predicted ratio  $|V_{ub}|/|V_{cb}|$  versus  $\sin 2\beta$  in  $M_d^{(5)}$ . The red dashed lines denote the upper and lower bounds of the experimental data with 90% C.L. in Eq. (16).

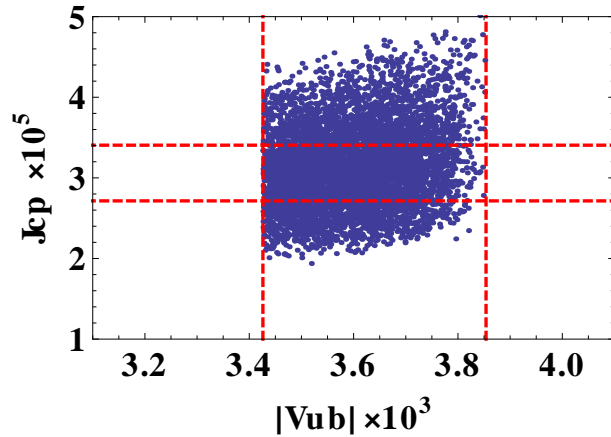


Figure 15: The predicted  $J_{CP}$  versus  $|V_{ub}|$  in  $M_d^{(5)}$ . The red dashed lines denote the upper and lower bounds of the experimental data with 90% C.L. in Eq. (16).

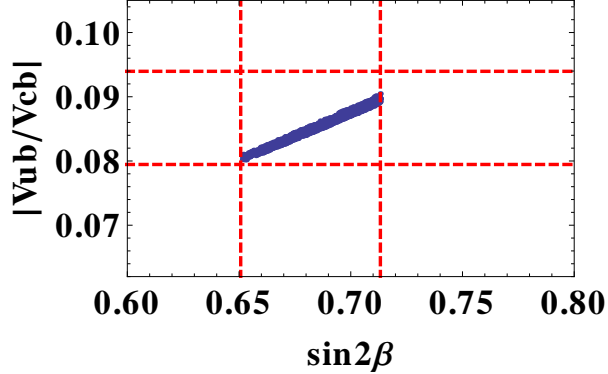


Figure 16: The predicted ratio  $|V_{ub}|/|V_{cb}|$  versus  $\sin 2\beta$  in  $M_d^{(11)}$ . The red dashed lines denote the upper and lower bounds of the experimental data with 90% C.L. in Eq. (16).

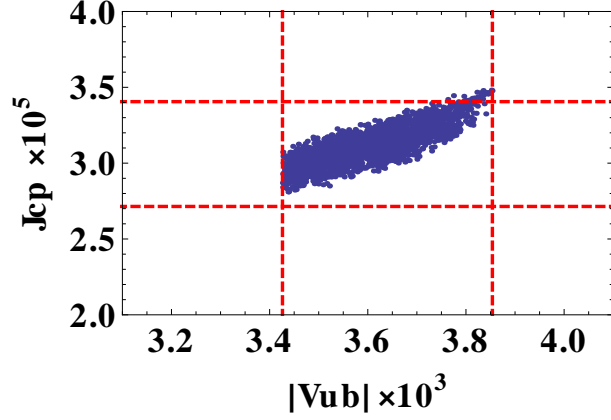


Figure 17: The predicted  $J_{CP}$  versus  $|V_{ub}|$  in  $M_d^{(11)}$ . The red dashed lines denote the upper and lower bounds of the experimental data with 90% C.L. in Eq. (16)

## 4 Discussions and Summary

In our work, we consider the minimum number of parameters of the quark mass matrices needed for the successful CKM mixing angles and the CP violation. We impose three zeros in the down-quark mass matrix by taking the diagonal up-quark mass matrix. The three zeros are maximal zeros to keep the CP violating phase in the quark mass matrix. Then, there remain six real parameters and one CP violating phase, which is the minimal number to reproduce the observed data of the down-quark masses and the CKM parameters. In order to reproduce the bottom-quark mass and the CKM mixing,  $V_{us}$  and  $V_{cb}$ , we take the (3, 3), (2, 3), (1, 2) elements of the  $3 \times 3$  down-quark mass matrix to be non-vanishing. Therefore, we have  ${}_6C_3 = 20$  textures with three zeros. We have found that the thirteen textures among twenty ones are viable for the down-quark mass matrix. They are classified into three groups in Table 1. It is remarked that these textures have freedoms of the unitary transformation of the right-handed quarks and some textures are transformed to other ones. By using such transformations, we have found that six textures are independent among the thirteen textures (see Appendix B).

As a representative of the above six textures, we have discussed the texture  $M_d^{(1)}$  in details to see how well the Cabibbo angle is predicted. By imposing the experimental data on  $\sin 2\beta$ ,  $\theta_{13}$  and  $\theta_{23}$ , the Cabibbo angle is predicted to be close to the experimental data. We have found that this surprising result remains unchanged in all other viable textures. Thus, the Occam's Razor approach is very powerful to obtain the successful Cabibbo angle.

After fixing all parameters by using the experimental data of three down-quark masses, the three CKM mixing angles and one CP violating phase, we have investigated the correlation between  $|V_{ub}/V_{cb}|$  and  $\sin 2\beta$ . For all textures, the maximal value of the ratio  $|V_{ub}/V_{cb}|$  is 0.09, which is smaller than the upper-bound of the experimental data, 0.094. We have also discussed  $J_{CP}$  versus  $|V_{ub}|$ . The predicted  $J_{CP}$  is almost the same among the first and third groups of Table 1, but different from the one in the second group. The precise data

$|V_{ub}/V_{cb}|$ ,  $J_{CP}$  and  $\sin 2\beta$  provide us the important test for our textures.

Our textures have been analyzed at the electroweak scale in this paper. The stability of texture zeros of the quark mass matrix has been examined against the renormalization-group evolution from the GUT scale to the electroweak scale by Xing and Zhao [11]. They found that texture zeros of the quark mass matrix are essentially stable against the evolution. Thus, we expect that the conclusions derived in this paper do not change much even if we consider the textures in Eqs.(4) and (6) at the GUT scale.

### **Acknowledgement**

This work is supported by JSPS Grand-in-Aid for Scientific Research (15K05045;M.T) and Scientific Research B (No.26287039;TTY). This work is also supported by World Premier International Research Center Initiative (WPI Initiative), MEXT, Japan.

## Appendix

### A Unfavored down-quark mass matrices

As discussed in the section 3, the four textures (seventh-tenth ones) in Eq.(3) are excluded by the experimental data. The following seventh, eighth and ninth textures are easily shown to be inconsistent with the experimental data:

$$M_d^{(7)} = \begin{pmatrix} 0 & a & 0 \\ a' & b e^{-i\phi} & c \\ c' & 0 & d \end{pmatrix}, \quad M_d^{(8)} = \begin{pmatrix} a' & a & 0 \\ c' & b e^{-i\phi} & c \\ 0 & 0 & d \end{pmatrix}, \quad M_d^{(9)} = \begin{pmatrix} 0 & a & c' \\ 0 & b e^{-i\phi} & c \\ 0 & a' & d \end{pmatrix}. \quad (19)$$

The both matrices  $M_d^{(7)} M_d^{(7)\dagger}$  and  $M_d^{(8)} M_d^{(8)\dagger}$  give the vanishing (13), (31) elements. These zeros are consistent only when  $\theta_{13} = 0$ ,  $\theta_{23} = 90^\circ$  or  $\delta_{CP} = 0$ . Actually, the Jarlskog invariant  $J_{CP}$  of those textures vanishes. The matrix  $M_d^{(9)}$  has one zero eigenvalue, that is, the lightest d-quark is massless.

The last texture in Eq.(3) is non-trivial one. We parametrize the texture as follows:

$$M_d^{(10)} = \begin{pmatrix} a' & a & 0 \\ 0 & b e^{-i\phi} & c \\ c' & 0 & d \end{pmatrix}, \quad (20)$$

which gives the CKM elements in the leading order as follows:

$$|V_{us}| \simeq 2 \frac{ab}{m_s^2} \left| \sin \frac{\phi}{2} \right|, \quad |V_{cb}| \simeq \frac{c}{m_b}, \quad |V_{ub}| \simeq \frac{a'c'}{m_b^2}, \quad \delta_{CP} \simeq \frac{1}{2}(\pi + \phi), \quad (21)$$

where we adopt the approximate relations  $a' \sim a$ ,  $c \sim 2b$  and  $c' \sim d$ . The  $J_{CP}$  is given as

$$J_{CP} = \frac{1}{(m_b^2 - m_s^2)(m_s^2 - m_d^2)(m_b^2 - m_d^2)} aa'bcc'd \sin \phi. \quad (22)$$

Therefore,  $\sin \phi$  should be positive. Then,  $\delta_{CP}$  is larger than  $90^\circ$  or negative, which is completely excluded by the experimental data in Eq.(16). Actually, we have obtained  $\delta_{CP} \geq 90^\circ$  under the experimental constraint of  $|V_{us}|$ ,  $|V_{cb}|$  and  $|V_{ub}|$  numerically.

The following textures (seventh-tenth ones) in Eq.(5) are also excluded by the experimental data:

$$M_d^{(18)} = \begin{pmatrix} a' & a e^{i\phi} & 0 \\ 0 & 0 & c \\ b & c' & d \end{pmatrix}, \quad M_d^{(19)} = \begin{pmatrix} 0 & a & 0 \\ a' & 0 & c \\ b & c' e^{-i\phi} & d \end{pmatrix}, \quad M_d^{(20)} = \begin{pmatrix} a' & a & 0 \\ b & 0 & c e^{i\phi} \\ 0 & c' & d \end{pmatrix}. \quad (23)$$

The both matrices  $M_d^{(18)} M_d^{(18)\dagger}$  and  $M_d^{(19)} M_d^{(19)\dagger}$  give the vanishing (12), (21) elements. These zeros are consistent only when  $\theta_{13} = 0$ ,  $\theta_{23} = 0$  or  $\delta_{CP} = 0$ . The Jarlskog invariant  $J_{CP}$  of those textures vanishes as well as  $M_d^{(7)}$  and  $M_d^{(8)}$ . Since  $M_d^{(20)}$  turns to  $M_d^{(10)}$  by the rotation of the right-handed quarks,  $M_d^{(20)}$  is excluded with the same reason of  $M_d^{(10)}$ ,  $\delta_{CP} \geq 90^\circ$ .

## B Redundancy of our textures

Since the CKM matrix is the flavor mixing among the left-handed quarks, the textures in Eqs.(4) and (6) have freedoms of the unitary transformation of the right-handed quarks. Under this transformation,  $M_d M_d^\dagger$  is invariant. We can easily seen that some textures are transformed to other ones as follows:

$$\begin{aligned} M_d^{(1)} &\equiv M_d^{(3)} , & M_d^{(2)} &\equiv M_d^{(16)} \equiv M_d^{(17)} , & M_d^{(4)} &\equiv M_d^{(5)} \equiv M_d^{(14)} , \\ M_d^{(11)} &\equiv M_d^{(13)} \equiv M_d^{(15)} , & M_d^{(10)} &\equiv M_d^{(20)} , \end{aligned} \quad (24)$$

where the notation " $\equiv$ " means the equivalent up to the unitary transformation of the right-handed quarks. In addition, we can easily see that  $M_d^{(7)}$ ,  $M_d^{(8)}$ ,  $M_d^{(18)}$  and  $M_d^{(19)}$  can be transformed to the textures with four zeros by the right-handed quark rotation. Therefore, these ones are excluded. In conclusion, we have viable six independent textures for the down-quark mass matrix.

## References

- [1] S. Weinberg, Trans. New York Acad. Sci. **38** (1977) 185.
- [2] R. Gatto, G. Sartori and M. Tonin, Phys. Lett. B **28** (1968) 128.
- [3] H. Fritzsch, Phys. Lett. B **73** (1978) 317.
- [4] H. Fritzsch, Nucl. Phys. B **155** (1979) 189.
- [5] P. Ramond, R. G. Roberts and G. G. Ross, Nucl. Phys. B **406** (1993) 19 doi:10.1016/0550-3213(93)90159-M [hep-ph/9303320].
- [6] K. Harigaya, M. Ibe and T. T. Yanagida, Phys. Rev. D **86** (2012) 013002 [arXiv:1205.2198 [hep-ph]].
- [7] M. C. Gonzalez, M. Malton and T. Schwetz, arXiv:1512.06856 [hep-ph].
- [8] K.A. Olive et al. (Particle Data Group), Chin. Phys. C, 38, 090001 (2014).
- [9] C. Jarlskog, Phys. Rev. Lett. **55** (1985) 1039.
- [10] S. Antusch and V. Maurer, JHEP **1311** (2013) 115 doi:10.1007/JHEP11(2013)115 [arXiv:1306.6879 [hep-ph]].
- [11] Z. z. Xing and Z. h. Zhao, Nucl. Phys. B **897** (2015) 302 doi:10.1016/j.nuclphysb.2015.05.027 [arXiv:1501.06346 [hep-ph]].